Surveys in Geophysics (2022) 43:1929–1945
https://doi.org/10.1007/s10712-022-09733-0

Short-Term Polar Motion Forecast Based on the Holt-Winters Algorithm and Angular Momenta of Global Surficial Geophysical Fluids

Jiesi Luo[1] · Wei Chen[1] · Jim Ray[2] · Jiancheng Li[1]

Received: 2 April 2022 / Accepted: 14 July 2022 / Published online: 16 August 2022

Abstract
By taking into account the variable free polar motion (PM) known as the Chandler wobble (CW) and irregular forced PM excited by quasi-periodic changes in atmosphere, oceans and land water (described by the data of effective angular momenta EAM), we propose a short-term PM forecast method based on the Holt-Winters (HW) additive algorithm (termed as the HW-VCW method, with VCW denoting variable CW). In this method, the variable CW period is determined by minimizing the differences between PM observations and EAM-derived PM for every 8-year sliding timespan. Compared to the X- and Y-pole forecast errors (ΔPMX and ΔPMY) of the International Earth Rotation and Reference Systems Service (IERS) Bulletin A, our results derived from operational EAM can reduce ΔPMX by up to 38.4% and ΔPMY by up to 34.3% for forecasts ranging from 1 to 30 days. Further, we prove that using EAM forecast instead of operational EAM in the HW-VCW method can achieve similar accuracies.

Keywords Earth orientation parameters · Polar motion forecast · Holt-Winters algorithm · Chandler wobble · Geophysical excitation

Highlights

- Holt-Winters additive algorithm is introduced into polar motion forecast for the first time
- Chandler Wobble variability is considered in polar motion forecast via variable Chandler period
- Our new method can improve polar motion forecast notably with enhanced geophysical significance

Retired: Jim Ray

✉ Wei Chen
wchen@sgg.whu.edu.cn

[1] Key Laboratory of Geospace Environment and Geodesy, School of Geodesy and Geomatics, Wuhan University, Wuhan 430079, China

[2] National Oceanic and Atmospheric Administration, Silver Spring, MD 20910, USA

1 Introduction

The rotational variations of the solid Earth, relative to the international celestial reference frame (ICRF) and the international terrestrial reference frame (ITRF), are defined by five Earth Orientation Parameters (EOPs), namely nutation, polar motion (PM) and changes in universal time ΔUT1, which can be accurately measured by advanced geodetic observation (e.g., Petit and Luzum 2010; Ratcliff and Gross 2010; Gross 2015; Ray 2016; Ray et al. 2017) and routinely released by the International Earth Rotation and Reference System Service (IERS) (Bizouard et al. 2019). While real-time EOPs are not available mainly due to delays in collecting and processing global data sets, they are of great significance for a number of practical applications, such as precise positioning, satellite navigation and satellite orbit determination (e.g., Ray et al. 2017; Wang et al. 2017). Therefore, accurate and efficient forecast of EOPs is urgently needed but a challenging task since PM, part of EOPs, contains not only the components excited by quasi-periodic mass redistributions and relative motions within the Earth system (Lambeck 1980; Jochmann 2009; Chen et al. 2013a, b; Gross 2015; Bizouard, 2020; Harker et al. 2021) but also the freely damping Chandler Wobble (CW) (Gross 2000, 2015; Schuh et al. 2001; Wang et al. 2016). These complexities can significantly degrade the accuracy of PM forecast.

For over three decades, PM has usually been predicted with harmonic analyses, least squares (LS), autoregressive (AR) and Kalman filter, etc., applied to accurate observations of recent past PM variations. (e.g., Javanović 1988; Freedman et al. 1994; Kosek et al. 1998; Gross et al. 1998; Akulenko et al. 2002a, b, c). By combining LS and AR, Kosek et al. (2008) put forward the LS + AR method. Xu et al. (2012) applied a Kalman filter prior to LS + AR, while Wu et al. (2018) used weighted LS + AR, both of which were proved to be effective, reducing mean absolute errors (MAE) of 1-day X- and Y-pole polar motion (PMX and PMY) forecasts to less than 0.3 mas (milli-arcsecond). Dobslaw and Dill (2018) and Dill et al. (2019) forecasted PM using effective angular momentum (EAM) and then adopted LS + AR to model unexplained residuals (named as EAM + LS + AR). The root-mean-square errors (RMSE) of their 1-day and 6-day PM forecasts are, respectively, within 0.2–0.4 mas and 0.9–1.5 mas, reduced, respectively, to 85.4% and 57.8% compared with the IERS bulletin A forecasts, validating the reliability of utilizing EAM products in PM prediction. Besides the widely adopted (revised) LS + AR method, Malkin and Miller (2010) and Modiri et al. (2018) proposed the use of singular spectrum analysis (SSA), Kosek et al. (2006) and Su et al. (2014) tried wavelet or normal time–frequency analysis, Schuh et al. (2002), Liao et al. (2012) and Wang et al. (2018) also used artificial neural networks. Zotov et al. (2018) predicted 90-day PM by combining LS, AR, LS collocation and artificial neural networks, in which weights are negatively correlated to respective PM prediction errors. Jin et al. (2021) used the multi-channel singular spectrum analysis (MSSA) method combining linear PM trend and autoregressive moving average to improve long-term PM forecast. Most of these PM forecast methods require either long PM timeseries or priori values of CW period T_{cw} and quality factor Q_{cw}, and thus predict long-time PM better rather than short-term PM.

Although the numerical value of Q_{cw} is poorly determined and varies significantly from study to study [for example, 63 of Jeffreys (1972); 88.4 of Mathews et al. (2002); 96 of Ooe (1978); 100 of Wilson and Haubrich (1976); 100.2 of Chen and Shen (2010); 127 of Nastula and Gross (2015); 179 of Wilson and Vicente (1990)], Q_{cw} is in fact dominated by mantle anelasticity (e.g., Lambeck 1980; Smith and Dahlen 1981; Chen et al. 2013a) which is determined by properties of mantle minerals and thus unlikely to change within

a relatively short time scale. On the contrary, many studies indicated that the "well-determined" T_{cw} may be variable (see Conclusions and Discussions for detailed discussions) (Chandler 1891; Iijima 1965; Proverbio et al. 1971; Carter 1981; Gao 1997; Höpfner 2003; Chen et al. 2009).

In this research, we propose a short-term PM forecast method based on the Holt-Winters (HW) additive algorithm to combine contributions from both the EAM and variable CW. This new method, termed as the HW-VCW for short, can determine T_{cw} (we assume Q_{cw} being stable as it is dominated by mantle anelasticity) from PM timeseries using an eight-year sliding window and then use them to model the short-time CW, and thus can model the non-excited part of PM better.

This study is arranged as follows. Data and method are introduced in Sects. 2 to 4, respectively. PM forecast results, including secular stability test during 1998–2020 and forecast test in 2021, are shown in Sect. 5. Conclusions and Discussions are given in Sect. 6.

2 Data

2.1 IERS Polar Motion Observation Data

The daily-sampled PM of IERS Earth orientation parameter product EOP 14 C04 (C04 for short) is obtained by combining measurements from independent space geodetic observation systems and released by the IERS with 30-day latency. The pole coordinates of EOP 14 C04 products are consistent with the International Terrestrial Reference Frame 2014 (ITRF2014). The IERS 14 C04 PM data are used as the truth reference to test our HW-VCW method.

IERS also provides the continuously updated product called Bulletin A, which contains not only quick-look daily EOP estimates by smoothing the observed data, but also EOP forecasts up to 365 days following the last day of data (see https://www.iers.org/IERS/EN/DataProducts/EarthOrientationData/eop.html for more details). The Bulletin A forecasts are to be compared with our PM forecasts in Sect. 5.

2.2 ESMGFZ Angular Momentum Products

The Earth System Modeling group at the Deutsches GeoForschungsZentrum (ESMGFZ) releases non-tidal effective angular momentum (EAM) products, including atmospheric, oceanic, hydrological and sea level angular momentum (AAM, OAM, HAM, SLAM), based on their global grid solutions of general circulation models (GCM) (Dobslaw et al. 2010). The ESMGFZ AAM is based on the European Centre for Medium-Range Weather Forecasts (ECMWF) operational analysis with inverted barometer correction applied and surface pressure tides subtracted. The ESMGFZ OAM is based on the Max-Planck-Institute for Meteorology Ocean Model (MPIOM) ocean model (Jungclaus et al. 2013) and forced by the ECMWF atmospheric pressure. The ESMGFZ HAM is based on the Land Surface Discharge Model (LSDM) hydrological model (Dill 2008), in which soil moisture, snow, surface water, and water in rivers and lakes are all considered. High-resolution geographic-information-system-based river networks are used in this model for higher accuracy of the spatial mass distribution. The ESMGFZ SLAM is derived to conserve the global mass based on a

global mean sea-level. In recent updates, loading, self-attraction and rotation deformation correction of the ocean are included. Therefore, the sum of the four EAM products presents the total excitation of polar motion caused by changes in geophysical fluids. The AAM and OAM are 3-h sampled, while the HAM and SLAM are 24-h sampled. All ESMGFZ EAM operational products (ESMGFZ EAM Op) are in radian and can be converted into polar motion excitations in arc-second (e.g., Gross 2015).

ESMGFZ also provides 6-day forecasts (Dobslaw and Dill 2018) and 90-day forecasts (Dill et al. 2019) of EAM products (ESMGFZ EAM F06 and ESMGFZ EAM F90), both of which are based on the same meteorological models of EAM products and routinely published every day. All ESMGFZ EAM datasets can be downloaded at https://rz-vm115.gfz-potsdam.de:8080/repository.

3 Formulas

3.1 Relationship Between PM and EAM

Time-dependent pole coordinates $p(t)$ consist of damping free PM $p_{free}(t)$ and excited PM $p_{exci}(t)$ caused by geophysical fluids. According to Lambeck (1980) (also see Chen et al. 2013b), the observed PM $p(t)$ can be divided into the free damping CW and the excited PM due to the total excitation $\chi(t)$:

$$\begin{cases} p(t) = p_{\text{free}}(t) + p_{\text{exci}}(t) \\ p_{\text{free}}(t) = A_0 e^{i\phi_0} e^{i\sigma_{cw}t} \\ p_{\text{exci}}(t) = -i\sigma_{cw} e^{i\sigma_{cw}t} \int_{-\infty}^{t} \chi(\tau) e^{-i\sigma_{cw}\tau} \mathrm{d}\tau \end{cases} \tag{1}$$

where A_0 and ϕ_0 are, respectively, the initial amplitude and phase angle of $p_{free}(t)$, and σ_{cw} is the angular frequency of Chandler wobble defined by its period T_{cw} and quality factor Q_{cw}:

$$\sigma_{cw} = 2\pi \frac{1}{T_{cw}} \left[1 + \frac{i}{2Q_{cw}} \right] \tag{2}$$

Using the EAMs described in Sect. 2.2, the excited PM can be obtained according to the last equation of Eq. (1). According to the frequency-domain Liouville's equation for polar motion (Chen et al. 2017), one can derive the geodetic (or observed) excitation by

$$\chi_{FFT}(f) = \frac{\sigma_{cw} - 2\pi f}{\sigma_{cw}} p_{FFT}(f) \tag{3}$$

where $p_{FFT}(f) = FFT(p(t))$ and $\chi_{FFT}(f) = FFT(\chi(t))$, and $FFT(p(t))$ means applying the Fast Fourier Transfer (FFT) to $p(t)$. In fact, Eq. (3) also illustrates that excitations and excited PM can be easily converted to each other in the frequency domain.

3.2 Holt-Winters Additive Method

The Holt-Winters (HW) additive method (Holt 2004; Winters 1960) is capable of modeling and predicting timeseries containing trend and roughly constant seasonality through exponential weighted moving averages. It is a series of algorithms proposed for industrial situation where mechanized inventory control and production scheduling require massive forecasts of sales and usage of individual products and materials (Winters 1960). In an exponential system based on sufficient data, new variables are derived by weighted-combining values from both last and current periods, leading to easy and flexible derivation of model and prediction. Besides, it responds more rapidly to sudden variations and depends less on the older data, which makes an exponential system suitable for short-term forecast based on recent information (Holt 2004). Detailed descriptions of the HW additive method can be found in some textbooks (e.g., Brockwell and Davis 2002; Hyndman and Athanasopoulos 2021).

In the HW additive algorithm, a discrete signal Y_t with rounded period T and length N can be modeled by the recursion formula:

$$\begin{cases} \tilde{Y}_t = a_{t-1} + b_{t-1} + c_{t-T}, t \in [T+2, N] \\ \tilde{Y}_t = Y_t, t \in [1, T+1] \end{cases} \tag{4}$$

where $\tilde{Y}_t$ is the HW model of Y_t. a_t, b_t and c_t are variable intercept, slope and seasonal factor determined by weighted combination of present and previous variables. The recursions and initial values of them are expressed as

$$\begin{cases} a_{T+1} = Y_{T+1} \\ a_t = \alpha\left(Y_t - c_{t-T}\right) + (1-\alpha)\left(a_{t-1} + b_{t-1}\right), t \in [T+2, N] \\ b_{T+1} = \left(Y_{T+1} - Y_1\right)/T \\ b_t = \beta\left(a_t - a_{t-1}\right) + (1-\beta) b_{t-1}, t \in [T+2, N] \\ c_t = Y_t - Y_1 - (t-1) b_{T+1}, t \in [1, T+1] \\ c_t = \gamma\left(Y_t - a_t\right) + (1-\gamma) c_{t-T}, t \in [T+2, N] \end{cases} \tag{5}$$

where α, β and γ are damping factors with values within the interval [0,1] and are estimated to minimize the difference between $\tilde{Y}_t$ and Y_t. By using Eq. (4) and (5), $\tilde{Y}_t$ modeled by Holt-Winters additive method can be iterated. Therefore, h-step forecast of Y_t can be expressed as

$$\tilde{Y}_{N+h} = a_N + h b_N + c_{N+h-(k+1)T} \tag{6}$$

where k is the integer part of $(h-1)/T$. More details about the HW additive method can be found in Sect. 9.3 of Brockwell and Davis (2002).

4 Algorithm of the HW-VCW Method

By using formulas mentioned in Sect. 3, we can make PM forecast by using the HW-VCW method proposed by this study. The HW-VCW method consists of two major procedures: One is the determination of T_{cw}, and the other is modeling the residuals

unexplained by the ESMGFZ EAMs (see Fig. 1 for the flowchart). The two steps are explained in detail below.

4.1 Determination of CW Period

To minimize the errors of PM forecast in the HW-VCW method, period and quality factor of Chandler Wobble (T_{cw} and Q_{cw}) corresponding to the eight-year-long PM timeseries for modeling should be determined first with the following steps (also see the box with red dashed line in Fig. 1).

STEP 1: We derive the observed polar motion excitation χ_{C04} PM in IERS EOP14C04 p_{C04} by using Eq. (3). Please notice that appropriate data extensions at both ends of p_{C04} are necessary to overcome the edge effects brought by frequency domain computation.

STEP 2: We derive C04 excited PM $p_{exci,C04}$ from χ_{C04} by using Eq. (1). Then, C04 free PM is determined by $p_{free,C04} = p_{C04} - p_{exci,C04}$.

STEP 3: Similar to STEP2, we derive ESMGFZ excited PM $p_{exci,ESMGFZ}$ from χ_{ESMGFZ}. Total ESMGFZ polar motion p_{ESMGFZ} can be expressed as $p_{ESMGFZ} = p_{free,C04} + p_{exci,ESMGFZ}$ since the free PM $p_{free,C04}$ should be independent from excitations within the modeling timespan.

STEP 4: We calculate the X- and Y-component standard deviation (SD) δ_{PMX} and δ_{PMY} of $p_{C04} - p_{ESMGFZ}$, respectively. According to Eq. (1) to (3), δ_{PMX} and δ_{PMY} are determined by the T_{cw} and Q_{cw}. Therefore, the objective function is defined as

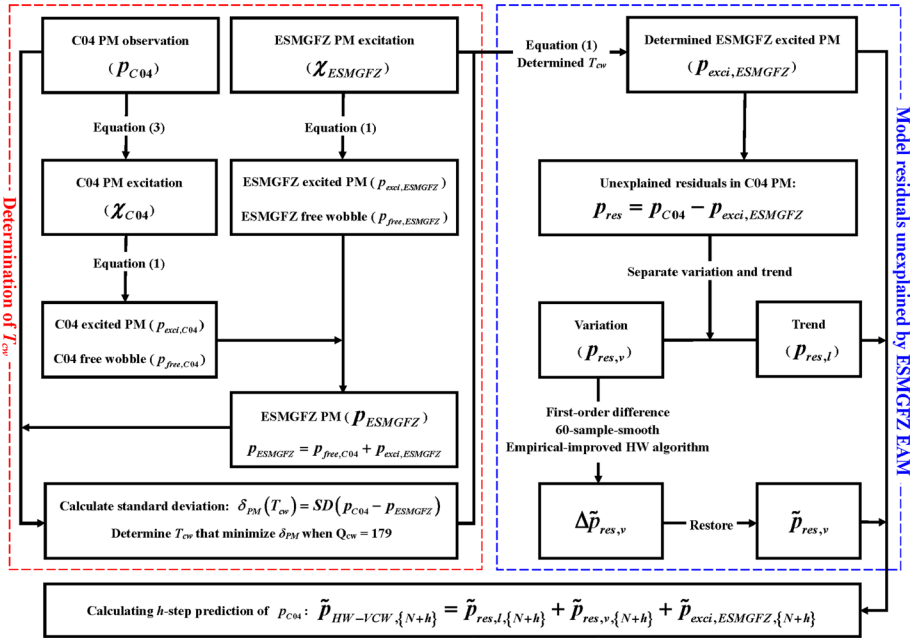

Fig. 1 Flowchart of PM forecast with the HW-VCW method. The procedure can be divided into two major parts: 1, determination of the T_{cw} that minimize the difference between C04 PM observation and ESMGFZ EAM-derived PM (denoted as ESMGFZ PM for short); 2, modeling of the residuals unexplained by ESMGFZ PM with the HW-VCW method. The two parts are marked with boxes with red and blue dashed lines, respectively

$$\delta_{PM}\left(T_{cw},Q_{cw}\right)=\sqrt{\delta_{PMX}\left(T_{cw},Q_{cw}\right)^2+\delta_{PMY}\left(T_{cw},Q_{cw}\right)^2} \tag{7}$$

$\delta_{PM}\left(T_{cw},Q_{cw}\right)$ represents the difference between observation $p_{IERS}(t)$ and model $p_{ESMGFZ}(t)$. Therefore, smaller $\delta_{PM}\left(T_{cw},Q_{cw}\right)$ means that T_{cw} and Q_{cw} used in STEP1–STEP3 are more reliable for the timespan.

STEP5: With initial CW period $T_0=433$ days, we use derivative-free fluctuated optimization in MATLAB to find the T_{cw} that minimizes $\delta_{PM}\left(T_{cw},Q_{cw}\right)$. This determined T_{cw} is regarded as the period of CW involved in the corresponding 8-year PM timeseries since it minimizes deviation between observed geodetic and modeled geophysical PM excitation function (Nastula and Gross 2015). However, we choose to adopt the constant value $Q_{cw}=179$ obtained by Wilson and Vicente (1990) and recommended by Gross (2015) in this research. That is because (1) Q_{cw} is mostly determined by properties of mantle minerals and unlikely to change within a relatively short time scale, as discussed in the Introduction; (2) our numerical tests indicate that while small Q_{cw} (e.g., $Q_{cw}<50$) will affect the EAM-derived PM significantly, the choice of Q_{cw} value hardly changes our PM forecast results for $Q_{cw}>100$.

4.2 Modeling the PM Residuals Unexplained by EAMs

By using the T_{cw} and Q_{cw} determined/adopted in Sect. 4.1, we can get the EAM-derived PM $p_{exci,ESMGFZ}$(this holds for both the ESMGFZ operational and forecast products). There is usually some difference between p_{C04} and $p_{exci,ESMGFZ}$, denoted as the residual unexplained by $p_{exci,ESMGFZ}$:

$$p_{res}=p_{C04}-p_{exci,ESMGFZ} \tag{8}$$

which can be separated into a linear trend $p_{res,l}$ and a nonlinear part $p_{res,v}$, which is dominated by the free damping CW according to Eq. (1), and can be predicted by the Holt-Winters algorithm.

The high-frequency components in $p_{res,v}$, such as daily fluctuations, will cause notable errors in short-term forecast using the Holt-Winters algorithm. Therefore, we model $\Delta p_{res,v}$, the 60-sample-smoothed first-order difference of $p_{res,v}$, instead of $p_{res,v}$ to reduce errors in PM forecast. The HW model of $\Delta p_{res,v}$ is established according to Eqs. (4) and (5). However, its h-step forecast $\Delta\tilde{p}_{res,v,\{N+h\}}$ is empirically modified from Eq. (6) to weaken the edge effect of parameters caused by numerical smoothing:

$$\Delta\tilde{p}_{res,v,\{N+h\}}=\begin{cases}\dfrac{a_{N-1}+a_N}{2}+\dfrac{b_{N-1}+b_N}{2}h+c_{N+h-(k+1)T},\ h=1\\ \dfrac{\sum_i^h a_{N-i+1}}{h}+\dfrac{\sum_i^h b_{N-i+1}}{h}h+c_{N+h-(k+1)T},\ h>1\end{cases} \tag{9}$$

where T is the nearest integer value of T_{cw}, while other parameters are defined the same as those in Eqs. (4) to (6). Therefore, the forecast of $p_{res,v}$ (represent by $\tilde{p}_{res,v}$) is restored as

$$\begin{cases}\tilde{p}_{res,v,\{N+1\}}=\Delta\tilde{p}_{res,v,\{N+1\}}+p_{res,v,\{N\}}\\ \tilde{p}_{res,v,\{N+h\}}=\Delta\tilde{p}_{res,v,\{N+h\}}+\tilde{p}_{res,v,\{N+h-1\}},\ h>1\end{cases} \tag{10}$$

(see the box with blue dashed line in Fig. 1).

With all relevant components obtained, the h-step (or h-day) PM forecast can be expressed as

$$\tilde{p}_{HW-VCW,\{N+h\}} = \tilde{p}_{res,l,\{N+h\}} + \tilde{p}_{res,v,\{N+h\}} + \tilde{p}_{exci,ESMGFZ,\{N+h\}} \tag{11}$$

according to Eq. (8). Here, $\tilde{p}_{res,l,\{N+h\}}$ is the predicted linear trend (namely the forecast of $p_{res,l}$), $\tilde{p}_{res,v,\{N+h\}}$ is calculated by Eq. (10), and $\tilde{p}_{exci,ESMGFZ,\{N+h\}}$ is derived from ESMGFZ forecast products using Eq. (1).

5 Results and Validations

The 30-day polar motion forecasts based on the HW-VCW method are illustrated and compared with the IERS EOP products and forecasts from some previous studies in this section.

In this study, 8-year-long IERS EOP14C04 and ESMGFZ EAM products before each forecast timespan are adopted to establish corresponding forecast models. However, the access to previous forecast products is unavailable since ESMGFZ online product repository preserves only the latest forecast products. Therefore, we separate the validation of the HW-VCW method into 2 parts: (1) Secular stability test, HW-VCW Op: January 1998 to December 2020: monthly and weekly 30-day forecast, in which ESMGFZ EAM Op are used to replace the inaccessible ESMGFZ EAM forecast products in forecast timespan. (2) Forecast test, HW-VCW F06: 22 September 2021 to 29 October 2021: daily 6-day forecast, in which ESMGFZ 6-day forecast products are used in forecast timespan.

5.1 Secular Stability Test

To test the stability of the HW-VCW method, we make 276 monthly 30-day polar motion forecasts starting from 2nd of each month during 1998–2020. Figure 2 shows the time-variable T_{cw} determined according to Sect. 3.2 for PM forecast. One can see that T_{cw} fluctuates within 426–436 days with an average 431.06 days, in accord with most previous studies (e.g., Jeffreys 1972; Wilson and Haubrich 1976; Ooe 1978; Wilson and Vicente 1990; Vicente and Wilson 1997; Guo et al. 2005).

Figure 3 shows monthly 30-day PM forecast error of HW-VCW Op relative to IERS EOP14C04 observation $\left(\Delta PM = \tilde{p}_{VC+HW} - p_{C04}\right)$ during Jan., 1998–Dec., 2020. In general, closer forecasts are more likely to be accurate and errors of Y-pole are significantly

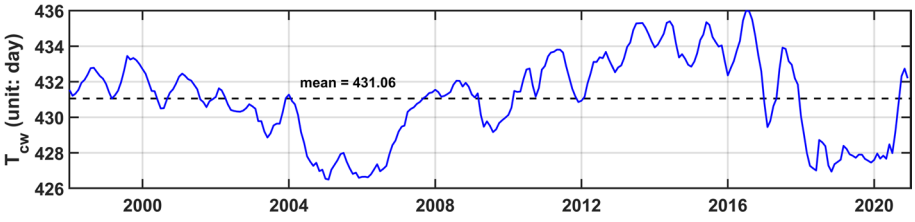

Fig. 2 Time-variable CW period (T_{cw}) for 30-day polar motion forecasts spanning January 1998 to December 2020 (276 monthly forecasts in total). T_{cw} are determined for every 8-year sliding timespan according to the method described in Sect. 3.2 with $Q_{cw}=179$. These T_{cw} values may not be very reliable (as they are determined using only 8-year data) but are efficient in improving PM forecasts

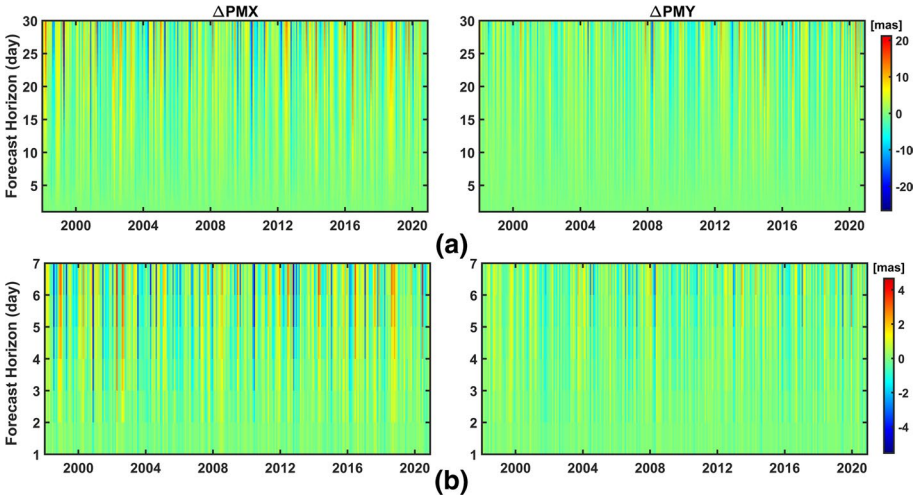

Fig. 3 Deviations between PM forecast derived by the HW-VCW method and IERS EOP14C04 polar motion observation during January 1998 to December 2020. **a** PMX and PMY forecast errors (ΔPMX and ΔPMX) up to 30 days, and **b** similar to **a** but for details up to 7-day forecast. Please notice that EAM operational products instead of forecast products are used for forecast in this figure

smaller than that of PMX. For the most important case 1-day forecast, 73.19% ΔPMX and 87.32% ΔPMY are smaller than 0.3 mas. When PMX and PMY are both considered, 59.42% ΔPM are smaller than 0.3 mas, and the root mean square errors (RMSE) is 0.34 mas for 1-day forecast, comparable to those of Dobslaw and Dill (2018) (0.35 mas), Dill et al. (2019) (0.40 mas), Schuh et al. (2002) (0.29 mas) and Chin et al. (2004) (0.29 mas).

Specifically, in Fig. 4, we compare absolute errors (AEs) and mean absolute errors (MAEs) of 1-, 5-, 10-, 20- and 30-day PM forecasts derived by HW-VCW Op with recent researches (Xu et al. 2012; Wu et al. 2018, 2021; Yao et al. 2013; Wang et al. 2018; Jin et al. 2021). Most AEs for the HW-VCW forecasts are smaller than MAEs of other researches in relative timespans. On day-1, MAEs of HW-VCW Op are 0.214 mas and 0.154 mas for PMX and PMY, while the best published results are 0.223 mas and 0.183 mas derived by weighted LS + AR (WLS + AR) (Wu et al. 2018). In forecasts up to day-30, our MAEs are still smaller than others, indicating that forecasts made by HW-VCW are reliable and stable within 30-day PM forecasts.

To further verify the HW-VCW method, we also make 828 weekly forecasts corresponding with IERS bulletin A products spanning 7 January 2005 to 20 November 2020. According to MAE listed in Table 1, by using the HW-VCW method, MAE of PMX forecast decreases by 20.00% while that of PMY forecasts decrease by 33.33% on day-1, reaching 0.24 and 0.16 mas, respectively. The HW-VCW method also improves 22.95–38.41% MAEs of PMX and 26.46–34.33% MAEs of PMY compared with Bulletin A within day-2–day-10. On day-20 and day-30, the HW-VCW method is still much better than Bulletin A in PMX forecasts with > 23% improvements achieved. However, PMY forecasts of Bulletin A perform much better than that of PMX during the same period, leading to decreasing MAE improvements of the HW-VCW method. In addition, please notice that Bulletin PM predition products have MAEs on day-0 (0.06 mas and 0.09 mas) caused by their combined EOP solution (slightly different from C04 EOP) spanning 6–8 days before the prediction horizon, which may enlarge the MAEs of Bulletin A PM prediction.

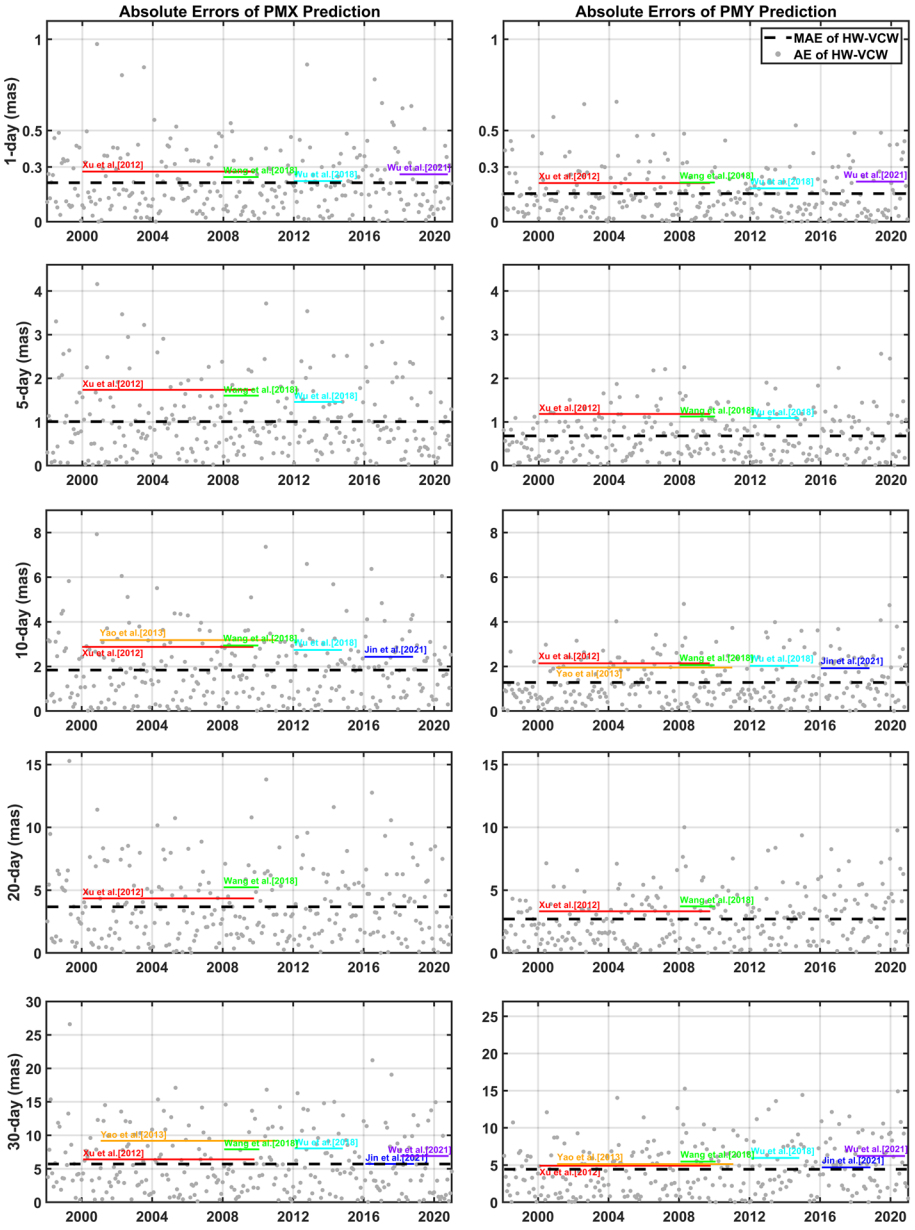

Fig. 4 Absolute errors (AEs) and mean absolute errors (MAEs) of 1-, 5-, 10-, 20- and 30-day PM forecasts spanning January 1998 to December 2020. Left: AE of PMX; Right: AE of PMY. Grey dots: AE of HW-VCW Op; Dashed black line: MAE of HW-VCW Op spanning January 1998 to December 2020; colored lines and texts: MAEs of other researches in their timespans given for comparison

5.2 Forecast Test

To test the HW-VCW method in real forecast and simulate the influences of the delay in

Table 1 Mean absolute error (MAE) of deviations between polar motion forecasts and IERS EOP14C04 EOP observation

Forecast horizon	ΔPMX			ΔPMY		
	Bulletin A	HW-VCW	Improvement	Bulletin A	HW-VCW	Improvement
Day-0	0.06	0	–	0.09	0	–
day-1	0.30	0.24	20.00%	0.24	0.16	33.33%
day-2	0.61	0.47	22.95%	0.44	0.30	31.82%
day-3	0.94	0.65	30.85%	0.67	0.44	34.33%
day-4	1.28	0.85	33.59%	0.89	0.59	33.71%
day-5	1.62	1.05	35.19%	1.09	0.74	32.11%
day-6	1.94	1.22	37.11%	1.28	0.88	31.25%
day-7	2.22	1.39	37.39%	1.44	1.01	29.86%
day-10	3.02	1.86	38.41%	1.89	1.39	26.46%
day-20	5.34	3.62	32.21%	3.31	2.87	13.29%
day-30	7.48	5.73	23.40%	4.74	4.69	1.05%

The HW-VCW method and IERS Bulletin A (weekly released products) are compared. Improvements of the HW-VCW method relative to Bulletin A results are also given. (Timespan: 7 January 2005 to 20 November 2020, Total: 828 weekly forecasts; Unit: mas)[a]

[a]Please notice that in secular test, we assume that C04 PM observation of day-0 is available (MAE of day-0 = 0 mas). However, for Bulletin A, day-0 MAEs exist due to the combined EOP used before forecast horizons

C04 release, we also compare the AEs of PM forecasts made by the HW-VCW F06 (using ESMGFZ EAM F06) with that of the HW-VCW Op (using ESMGFZ EAM Op) during 22 September 2021 to 29 October 2021 (their AE differences are determined as $\Delta AE = AE_{F06} - AE_{Op}$).

Assuming we have real-time access of PM observation data (namely, C04 release delay = 0 day), according to Fig. 5, PM predicted by the HW-VCW F06 is similar to that of ESMGFZ EAM F06 on day-1 and day-2 with most $\Delta AE < 0.1$ mas, while larger ΔAE appears on day-3 to day-6. However, it can be seen from the MAE curves in Fig. 5 and L0 vs. E0 in Table 2 that, for PMX and PMY, $MAEs_{F06}$ are almost the same as $MAEs_{Op}$ on day-1 to day-3 while 0.02–0.06 mas smaller than $MAEs_{Op}$ on day-4 to day-6, indicating that the HW-VCW F06 is even slightly better than the HW-VCW OP in this duration. Therefore, we infer that utilizing ESMGFZ EAM F06 instead of ESMGFZ EAM Op in the HW-VCW method will not significantly affect the accuracy of ultra-short PM forecast.

For the actual case that there is C04 release delay, most PM prediction methods are forced to make traditional multiple-day PM prediction (similar to L0 in Table 2). However, HW-VCW method has another option (L1–L6 in Table 2) by involving the latest EAM operational products if the daily released ESMGFZ EAM operational products are published on time. In this situation, excited PM of the delay days can be estimated from the available ESMGFZ EAM operational instead of forecast products. Delays of PM observation not only introduce deviations on day-0 but also enlarge MAEs of HW-VCW method on the same prediction day due to the extended prediction of free PM. Compared with non-delay conditions by calculating L6–L0 in Table 2, 6-day delay of C04 increases MAEs of PMX and PMY by 1.30–0.95 mas and 0.79–1.25 mas separately on prediction day-1 to day-6. Besides, we find that MAEs in Table 2 are generally descending from bottom-right to

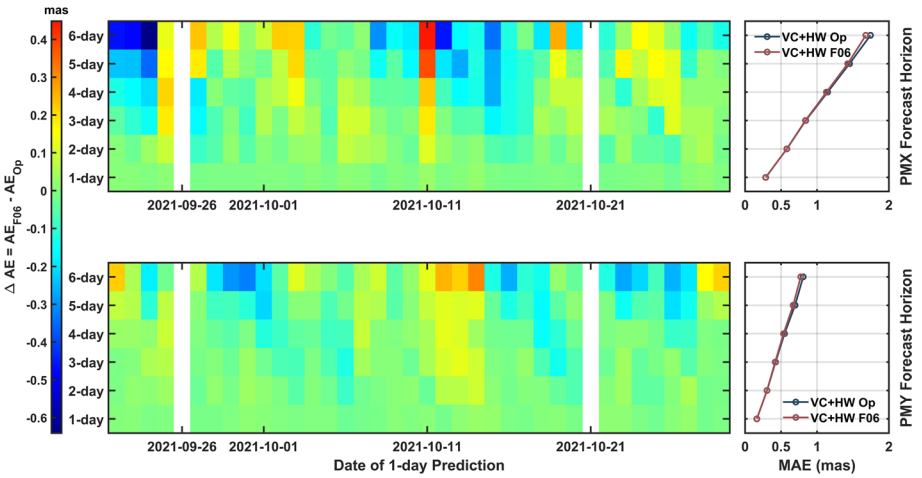

Fig. 5 Differences between 6-day PM absolute errors predicted by the HW-VCW Op and the HW-VCW F06 ($\Delta AE = AE_{F06} - AE_{Op}$) spanning 22 September 2021 to 29 October 2021 (36 forecasts in total). (left): ΔAEs of PMX and PMY, sharing the same color bar. Each rectangle presents the ΔAE on that day; (right): corresponding MAEs on each forecast days within 6-day forecast horizon (*y*-axis). (ESMGFZ EAM F06 on 26 September 2021 to 21 October 2021 were not available for download.)

top-left, corresponding to PM prediction results with longer delays but shorter prediction distances in L0–L6. For example, MAE of 1-day PMX prediction in L5 (1.47 mas) is smaller than other MAEs along its diagonal and significantly better than 1.68 mas of 6-day PMX prediction in L0. When the sums of delay and prediction steps are the same, L0–L6 have to predict free PM from the same distance. However, in L1–L6, parts of excited PM are calculated from EAM operational products, which is totally predicted by EAM forecast products in L0. Similar features of RMSE variations can also be found in Dobslaw and Dill (2018). Therefore, we infer that accuracy of HW-VCW method can be further improved by involving the latest ESMGFZ EAM operational products when PM observation is delayed in real PM forecast.

6 Discussion and Conclusions

Based on the Holt-Winters (HW) additive algorithm, we have proposed a new short-term PM forecast method HW-VCW, which can handle the variability of CW and take advantage of GCM-derived angular momentum products, and thus improve the accuracy of PM forecasts. The HW-VCW method is tested with both the IERS EOP C04 PM observation and Bulletin A PM forecast for its secular stability and then applied to real PM forecasts using ESMGFZ EAM 6-day forecast products. Our results show that the HW-VCW method is stable and reliable in different timespans and can bring 20.00–38.41% improvements in ΔPMX and 1.05–34.33% improvements in ΔPMY from 1 to 30 days into the future compared with PM forecasts in IERS bulletin A, from the aspect of MAE. Besides, we also proved that HW-VCW method is effective in real PM forecasts, in which case there is certain C04 release delay. Especially, the day-0 ESMGFZ EAM operational products contribute significantly in reducing the forecast MAE. Thus, the ESMGFZ EAM operational and forecast products are very beneficial for PM forecasts.

Table 2 MAE of polar motion predicted by the HW-VCW F06 and the HW-VCW Op relative to IERS EOP14C04 EOP observation (MAE_{F06} and MAE_{OP})

ID	EAM	C04 delay (days)	Day-0	Day-1	Day-2	Day-3	Day-4	Day-5	Day-6
MAE of PMX (unit: mas)									
L6	F06	−6	1.40	1.59	1.82	2.06	2.29	2.48	2.63
L5	F06	−5	1.23	1.47	1.66	1.91	2.15	2.37	2.57
L4	F06	−4	0.98	1.22	1.45	1.65	1.91	2.15	2.36
L3	F06	−3	0.76	1.04	1.28	1.51	1.73	1.98	2.21
L2	F06	−2	0.54	0.79	1.08	1.35	1.59	1.82	2.1
L1	F06	−1	0.28	0.56	0.83	1.15	1.42	1.68	1.88
L0	**F06**	**0**	**0**	**0.29**	**0.58**	**0.84**	**1.13**	**1.43**	**1.68**
E0	**OP**	**0**	**0**	**0.29**	**0.58**	**0.84**	**1.15**	**1.45**	**1.74**
MAE of PMY (unit: mas)									
L6	F06	−6	0.73	0.79	0.82	0.88	0.97	1.11	1.25
L5	F06	−5	0.6	0.72	0.78	0.81	0.87	0.95	1.08
L4	F06	−4	0.47	0.62	0.76	0.83	0.86	0.91	1
L3	F06	−3	0.37	0.49	0.64	0.77	0.84	0.88	0.96
L2	F06	−2	0.26	0.38	0.5	0.65	0.77	0.81	0.84
L1	F06	−1	0.15	0.28	0.4	0.53	0.67	0.77	0.82
L0	**F06**	**0**	**0**	**0.16**	**0.3**	**0.42**	**0.53**	**0.67**	**0.77**
E0	**OP**	**0**	**0**	**0.16**	**0.31**	**0.42**	**0.55**	**0.69**	**0.81**

In real forecast tests using ESMGFZ EAM forecast products, 6-day to 0-day delays of C04 PM observation are considered (Timespan: 22 September 2021 to 29October 2021, Total: 36 forecasts; Unit: mas)[a]

[a]In this table, 'ID' column listed code names of different experiments, which are used in the main text for conciseness. Day-0 MAEs of L0 and E0 are 0 because we assume that C04 publication is not delayed in both cases,

And these lines are in bold to emphasize them as our main prediction results. Other lines are not in bold as these consider cases of variable delays in C04 publication.

In the development of the HW-VCW PM forecast method, we have used the integration as expressed by Eq. (1) rather than the frequency-domain conversion as expressed by Eq. (3), since the possible noises and errors within the CW frequency band of excitations caused by observation or modelling (e.g., Zotov 2020) may be amplified.

In addition, we have assumed T_{cw} being variable since long-time observations show that T_{cw} may be time dependent. Chandler (1891) first suggested T_{cw} might be not only variable but also positively correlated with the CW amplitude. Iijima (1965) analyzed the International Latitude Service (ILS) data for the period 1900.0–1963.2 with a 0.1-year sampling and found that the T_{cw} varies from about 1.1 to 1.2 years and the smaller period happens when the CW has a smaller amplitude, and vice versa. Later, Proverbio et al. (1971) confirmed the correlation between the amplitudes and periods of the CW. Carter (1981) proposed a frequency modulation model to explain variations of both the amplitude and frequency of the CW and suggested that the nonequilibrium ocean pole tide can vary with time and lead to the frequency modulation of CW. Gao (1997) concluded that T_{cw} might have a 10-day fluctuation in correlation with CW amplitude during the last several decades. Höpfner (2003) found that the Chandler wobble has a period variation between 422 and 438 days with an estimated standard deviation of only 0.48 days, while its amplitude varies from 150 to 200 mas with a temporal dependence similar to the period. Based on the Jacobian elliptic functions, Chen et al. (2009) derived a theoretical model for the

frequency-amplitude modulation of the CW, which indicates T_{cw} is time dependent and can be affected by the CW amplitude.

Physically speaking, if the Earth is a body with fixed size, figure and density distribution, the CW frequency, as a normal mode or eigenfrequency of the Earth, would be a constant. However, as is well known, the Earth is undergoing continuous deformations (namely changing figure and density distribution) due to loading and tidal attractions, etc. Therefore, the normal mode CW frequency must be changing correspondingly, and the traditionally referred "observed CW frequency (or period)" should be understood as the mean value over a certain period. To conclude, T_{cw} can change with time though the amplitude of fluctuation is still uncertain.

Finally, the HW-VCW method developed in this study is most suitable for short-term PM forecast, as its forecast errors increase notably beyond 30 days in the future. However, one may extend the HW-VCW method to middle-term or even long-term PM forecast by improving the algorithms involved.

Acknowledgements Dr. Henryk Dobslaw and an anonymous reviewer are highly appreciated for their insightful comments and suggestions that helped to improve this study. We thank all the researchers that have collaborated in processing and publishing IERS EOP and ESMGFZ EAM products.

Funding This work was supported by the National Natural Science Foundation of China (Grant Numbers 41874025, 41474022).

Data Availability The IERS 14 C04 EOP data are available at https://datacenter.iers.org/data/, and the ESMGFZ EAM data can be accessed at http://rz-vm115.gfz-potsdam.de:8080/repository.

Declarations

Conflict of interest The authors declare no conflict of interest.

References

Akulenko LD, Kumakshev SA, Markov YuG (2002a) Motion of the Earth's pole. Dokl Phys 47:78–84. https://doi.org/10.1134/1.1450668

Akulenko LD, Kumakshev SA, Markov YuG, Rykhlova LV (2002b) A model for the polar motion of the deformable Earth adequate for astrometric data. Astron Rep 46:74–82. https://doi.org/10.1134/1.1436207

Akulenko LD, Kumakshev SA, Markov YuG, Rykhlova LV (2002c) Forecasting the polar motions of the deformable Earth. Astron Rep 46:858–866. https://doi.org/10.1134/1.1515097

Bizouard C (2020) Geophysical modelling of the polar motion. De Gruyter, Berlin. https://doi.org/10.1515/9783110298093

Bizouard C, Lambert S, Gattano C, Becker O, Richard J (2019) The IERS EOP14C04 solution for Earth orientation parameters consistent with ITRF 2014. J Geodesy 93(85):621–633. https://doi.org/10.1007/s00190-018-1186-3

Brockwell PJ, Davis RA (2002) Introduction to time series and forecasting, 2nd edn. Springer, New York
Carter WE (1981) Frequency modulation of the Chandlerian component of polar motion. J Geophys Res 86:1653–1658. https://doi.org/10.1029/JB086iB03p01653
Chandler SC (1891) On the variation of the latitude. Astron J 11:83–86
Chen W, Shen W (2010) New estimates of the inertia tensor and rotation of the triaxial nonrigid Earth. J Geophys Res 115:B12419. https://doi.org/10.1029/2009JB007094
Chen W, Shen W, Han J, Li J (2009) Free wobble of the triaxial Earth: theory and comparisons with International Earth Rotation Service (IERS) data. Surv Geophys 30:39–49. https://doi.org/10.1007/s10712-009-9057-3
Chen W, Ray J, Li JC, Huang C, Shen W (2013a) Polar motion excitations for an Earth model with frequency-dependent responses: 1. A refined theory with insight into the Earth's rheology and core-mantle coupling. J Geophys Res 118:4975–4994. https://doi.org/10.1002/jgrb.50314
Chen W, Ray J, Shen W, Huang C (2013b) Polar motion excitations for an Earth model with frequency-dependent responses: 2. Numerical tests of the meteorological excitations. J Geophys Res 118:4995–5007. https://doi.org/10.1002/jgrb.50313
Chen W, Li JC, Ray J, Cheng MK (2017) Improved geophysical excitations constrained by polar motion observations and GRACE/SLR time-dependent gravity. Geodesy Geodyn 6:11–22. https://doi.org/10.1016/j.geog.2017.04.006
Chin TM, Gross RS, Dickey JO (2004) Modeling and forecast of the polar motion excitation functions for short-term polar motion prediction. J Geodesy 78:343–353. https://doi.org/10.1007/s00190-004-0411-4
Dill R (2008) Hydrological model LSDM for operational Earth rotation and gravity field variations. GFZ Scientific Technical Report STR08/09
Dill R, Dobslaw H, Thomas M (2019) Improved 90-day Earth orientation predictions from angular momentum forecasts of atmosphere, ocean, and terrestrial hydrosphere. J Geodesy 93:287–295. https://doi.org/10.1007/s00190-018-1158-7
Dobslaw H, Dill R (2018) Predicting Earth orientation changes from global forecasts of atmosphere-hydrosphere dynamics. Adv Space Res 61(4):1047–1054. https://doi.org/10.1016/j.asr.2017.11.044
Dobslaw H, Dill R, Groetzsch A, Brzezinski A, Thomas M (2010) Seasonal polar motion excitation from numerical models of atmosphere, ocean, and continental hydrosphere. J Geophys Res 115:B10406. https://doi.org/10.1029/2009JB007127
Freedman AP, Steppe JA, Dickey JO, Eubanks TM, Sung LY (1994) The short-term prediction of universal time and length of day using atmospheric angular momentum. J Geophys Res 99:6981–6996. https://doi.org/10.1029/93JB02976
Gao BX (1997) Principles of astro-geodynamics. Scientific and Technological Press of China, Beijing
Gross RS (2000) The excitation of the Chandler wobble. Geophys Res Lett 27(15):2329–2332. https://doi.org/10.1029/2000GL011450
Gross RS (2015) Earth rotation variations-long period. In: Schubert G (ed) Treatise on geophysics, 2nd edn. Elsevier, New York, pp 215–261
Gross RS, Eubanks TM, Steppe JA, Freedman AP, Dickey JO, Runge TF (1998) A Kalman-filter-based approach to combining independent Earth orientation series. J Geodesy 72:215–235. https://doi.org/10.1007/s001900050162
Guo J, Greiner-Mai H, Ballani L, Jochmann H, Shum CK (2005) On the double-peak spectrum of the Chandler wobble. J Geodesy 78:654–659. https://doi.org/10.1007/s00190-004-0431-0
Harker AA, Schindelegger M, Ponte RM, Salstein DA (2021) Modeling ocean-induced rapid Earth rotation variations: an update. J Geodesy 95:110. https://doi.org/10.1007/s00190-021-01555-z
Holme R, de Viron O (2013) Characterization and implications of intradecadal variations in length of day. Nature 499:202–204. https://doi.org/10.1038/nature12282
Holt CC (2004) Forecasting seasonals and trends by exponentially weighted moving averages. Int J Forecast 20:5–10. https://doi.org/10.1016/j.ijforecast.2003.09.015
Höpfner J (2003) Chandler and annual wobbles based on space-geodetic measurements. J Geodyn 36(3):369–381. https://doi.org/10.1016/S0264-3707(03)00056-5
Hyndman RJ, Athanasopoulos G (2021) Forecasting: principles and practice, 3rd edn. Melbourne, OTexts
Iijima S (1965) On the yearly trend of the periodic components of polar motion. Ann Tokyo Astron Obs 9:155–181
Javanović B (1988) An analytical representation of ephemeris data. Celest Mech 45:317–320. https://doi.org/10.1007/BF01229016
Jeffreys H (1972) The variation of latitude. In: Melchior P, Yumi S (eds) Rotation of the Earth. D. Reidel, Dordrecht, pp 39–42

Jin X, Liu X, Guo J, Shen Y (2021) Analysis and prediction of polar motion using MSSA method. Earth Planets Space 73:147. https://doi.org/10.1186/s40623-021-01477-2

Jochmann H (2009) Basic relations for studying the influence of geophysical processes on the Earth's rotation: the angular momentum approach. Surv Geophys 30:1–37. https://doi.org/10.1007/s10712-009-9056-4

Jungclaus JH, Fischer N, Haak H, Lohmann K, Marotzke J, Matei D, Mikolajewicz U, Notz D, von Storch JS (2013) Characteristics of the ocean simulations in the Max Planck Institute Ocean Model (MPIOM) the ocean component of the MPI-Earth system model. J Adv Model Earth Syst 5:422–446. https://doi.org/10.1002/jame.20023

Kosek W, McCarthy DD, Luzum BJ (1998) Possible improvement of Earth orientation forecast using autocovariance prediction procedures. J Geodesy 72:189–199. https://doi.org/10.1007/s001900050160

Kosek W, Rzeszótko A, Popinski W (2006) Phase variations of oscillations in the Earth orientation parameters detected by the wavelet technique. In: Proceedings of the journèes 2005 systèmes de référence spatio-temporels, pp 121–124.

Kosek W, Kalarus M, Niedzielski T (2008) Forecasting of the Earth orientation parameters comparison of different algorithms. In: Capitaine, N. (Ed.), Proceedings of the Journèes 2007, systèmes deréférence spatio-temporels The celestial reference frame for the future. Observatoire de Paris Systèmes de Référence Temps-Espace UMR8630/CNRS. Paris, France, pp. 155–158.

Lambeck K (1980) The Earth's variable rotation: geophysical causes and consequences. Cambridge University Press, New York

Liao D, Wang Q, Zhou Y, Liao X, Huang C (2012) Long-term prediction of the earth orientation parameters by the artificial neural network technique. J Geodyn 62:87–92. https://doi.org/10.1016/j.jog.2011.12.004

Malkin Z, Miller N (2010) Chandler wobble: two more large phase jumps revealed. Earth Planets Space 62(12):943–947. https://doi.org/10.5047/eps.2010.11.002

Mathews PM, Herring TA, Buffett BA (2002) Modeling of nutation and precession: new nutation series for nonrigid Earth and insights into the Earth's interior. J Geophys Res 107(B4):2068. https://doi.org/10.1029/2001JB000390

Modiri S, Belda S, Heinkelmann R, Hoseini M, Ferrándiz JM, Schuh H (2018) Polar motion prediction using the combination of SSA and Copula-based analysis. Earth Planets Space 70:115. https://doi.org/10.1186/s40623-018-0888-3

Nastula J, Gross R (2015) Chandler wobble parameters from SLR and GRACE. J Geophys Res 120:4474–4483. https://doi.org/10.1002/2014JB011825

Ooe M (1978) An optimal complex AR.MA model of the Chandler wobble. Geophys J Roy Astron Soc 53:445–457. https://doi.org/10.1111/j.1365-246X.1978.tb03752.x

Petit G, Luzum B (2010) IERS Conventions (2010). (IERS Technical Note ; 36) Frankfurt am Main: Verlag des Bundesamts für Kartographie und Geodäsie, 2010. 179 pp., ISBN 3–89888–989–6

Proverbio E, Carta F, Mazzoleni F (1971) Analysis of the Chandler period of polar coordinates calculated-with Orlov's method, Pubblicazioni Della Stazione Astronomica Internazionale Di Latitudine Carloforte-Cagliari. Nuova Serie N. 18

Ratcliff JT, Gross RS (2010) Combinations of Earth orientation measurements: SPACE2008, COMB2008, and POLE2008. JPL Publ 10–4:1–27

Ray J (2016) Precision, accuracy, and consistency of GNSS products. In: Grafarend EW (ed) Encyclopedia of Geodesy. Springer, Geneva

Ray J, Rebischung P, Griffiths J (2017) IGS polar motion measurement accuracy. Geodesy Geodyn 8:413–420. https://doi.org/10.1016/j.geog.2017.01.008

Schuh H, Nagel S, Seitz T (2001) Linear drift and periodic variations observed in long time series of polar motion. J Geodesy 74(10):701–710

Schuh H, Ulrich M, Egger D, Muller J, Schwegmann W (2002) Prediction of Earth orientation parameters by artificial neural networks. J Geodesy 76:247–258. https://doi.org/10.1007/s00190-001-0242-5

Smith ML, Dahlen FA (1981) The period and Q of the Chandler wobble. Geophys J Int 64(1):223–281. https://doi.org/10.1111/j.1365-246X.1981.tb02667.x

Su X, Liu L, Houtse H, Wang G (2014) Long-term polar motion prediction using normal time–frequency transform. J Geodesy 88:145–155. https://doi.org/10.1007/s00190-013-0675-7

Vicente RO, Wilson CR (1997) On the Variability of the chandler frequency. J Geophys Res 102(B9):20439–20445. https://doi.org/10.1029/97JB01275

Wahr JM (1983) The effects of the atmosphere and oceans on the Earth's wobble and on the seasonal variations in the length of day—II Results. Geophys J Int 74(2):451–487. https://doi.org/10.1111/j.1365-246X.1983.tb01885.x

Wang G, Liu L, Su X, Liang X, Yan H, Tu Y, Li Z, Li W (2016) Variable chandler and annual wobbles in Earth's polar motion during 1900–2015. Surv Geophys 37(6):1075–1093. https://doi.org/10.1007/s10712-016-9384-0

Wang Q, Hu C, Xu T, Chang G, Moraleda AH (2017) Impacts of Earth rotation parameters on GNSS ultra-rapid orbit prediction: derivation and real-time correction. Adv Space Res 60(12):2855–2870. https://doi.org/10.1016/j.asr.2017.09.022

Wang G, Liu L, Tu Y, Xu X, Yuan Y, Song M, Li W (2018) Application of the radial basis function neural network to the short term prediction of the Earth's polar motion. Stud Geophys Geod 62:243–254. https://doi.org/10.1007/s11200-017-0805-4

Wilson CR, Haubrich RA (1976) Meteorological excitation of the Earth's wobble. Geophys J Roy Astron Soc 46:707–743. https://doi.org/10.1111/j.1365-246X.1976.tb01254.x

Wilson CR, Vicente RO (1990) Maximum likelihood estimates of polar motion parameters. In: McCarthy DD, Carter WE (eds) Variations in Earth rotation. American Geophysical Union Geophysical Monograph Series, Washington

Winters PR (1960) Forecasting sales by exponentially weighted moving averages. Manage Sci 6(3):324–342. https://doi.org/10.1287/mnsc.6.3.324

Wu F, Deng K, Chang G, Wang Q (2018) The application of a combination of weighted least-squares and autoregressive methods in predictions of polar motion parameters. Acta Geod Geoph 53:247–257. https://doi.org/10.1007/s40328-018-0214-3

Wu F, Liu Z, Deng K, Chang G (2021) A polar motion prediction method considering the polar coordinates. Adv Space Res 68:1318–1328. https://doi.org/10.1016/j.asr.2021.03.020

Xu X, Zhou Y, Liao X (2012) Short-term earth orientation parameters predictions by combination of the least-squares, AR model and Kalman filter. J Geodyn 62:83–86. https://doi.org/10.1016/j.jog.2011.12.001

Yao Y, Yue S, Chen P (2013) A new LS+AR model with additional error correction for polar motion forecast. Sci China Earth Sci 56(5):818–828. https://doi.org/10.1007/s11430-012-4572-3

Zotov LV, Xu XQ, Skorobogatov A, Zhou YH (2018) Combined SAI-SHAO prediction of Earth orientation parameters since 2012 till 2017. Geodesy Geodyn 9(6):818–828. https://doi.org/10.1016/j.geog.2018.11.002

Zotov LV, Bizouard C, Sidorenkov N, Shen WB, Guo ZL (2020) On the variability of the Chandler wobble. Proceedings of Journées 2019. pp 249–254. https://ui.adsabs.harvard.edu/abs/2020jsrs.conf..249Z/abstract